JOURNAL OF SPACECRAFT AND ROCKETS
Vol. 38, No. 6, November–December 2001

Interactions Between a Canard and Thick Bodies: Analysis and Applications

Asher Sigal*
San Diego State University, San Diego, California 92182-1308

A modular model, consisting of cruciform canard controls mounted on a thin forebody and five interchangeable thick (larger-diameter) main bodies, was tested at a Mach number of 0.8. The canard was installed at the + and x positions and at deflection angles of 0, 6, and 12 deg. The model was equipped with two sting balances in a setup that enabled to obtain the loads acting on the canard unit and those acting on the main bodies. Four interactions on main body normal force and center of pressure are identified and quantified: effects of the canard on the thickening of the main bodies and on the boattails, as a function of angle of attack and canard deflection. The interactions are analyzed using an approximate vortex tracker, which is based on slender body theory. Then, the pertinent part of the Pitts, Nielsen, and Kaattari component buildup method is used to calculate the interactions. The results of the analysis are in good agreement with the present test data, except for the effect of canard deflection on the boattail, where the analysis leaves a large gap. Using the present method, to add the subject effects to component buildup analysis of variety of configurations improves the agreement with test data.

Nomenclature

B = main body
b = forebody
bt = boattail
C = canard
C_L = lift coefficient
C_{L_α} = lift curve slope
C_m = pitching-moment coefficient
C_{m_α} = pitching-moment curve slope
C_N = normal-force coefficient
C_{N_α} = normal-force curve slope
c = side of a square base
D = diameter of main body, mm
d = reference length, diameter of the forebody, mm
d_{be} = equivalent base diameter
f = lateral position of a trailing vortex
g = lateral position of an image vortex
h = vertical position of a trailing vortex
h_i = vertical position of an image vortex
I = influence factors, defined by Eqs. (2–5)
L = lift force
l = moment arm
M = Mach number
q_r = radial velocity component in the transverse plane
R = radial coordinate in the transverse plan
r = body radius
S = body cross-sectional area
S_R = reference area, $(\pi/4)d^2$, mm^2
U = freestream velocity
x_{cp} = center-of-pressure location
α = angle of attack
Γ = circulation
δ = canard deflection
ρ = air density
σ = strength of source

Subscripts

f = front balance
m = main balance
1 = thickening of main body

Introduction

THE first part of this paper, Ref. 1, describes a wind-tunnel investigation of a modular model, consisting of a canard unit mounted on a thin forebody and five interchangeable thick main bodies. Reference 1 gives the geometry of the model and the test conditions and describes the measurement system. It emphasizes the aerodynamic characteristics of the bodies alone and of the canard unit. It also identifies the effects of the main bodies on the canards: a slight decrease of the normal-force curve slope and of the normal force caused by canard deflection, as main body thickness increases.

The objectives of this part of the study are 1) to identify and quantify the effects of the canards on the thickenings of the main bodies (the ogives connecting the forebody to the main bodies) and on the boattails; 2) to analyze these effects; 3) to add the present analysis to component buildup calculation of the longitudinal and control characteristics of several configuration; and 4) to compare the results with available test data and evaluate applicability for design.

Interactions

Models and Tests

A schematic of the test model and the measurement system are depicted in Figs. 1 and 2. This arrangement provided the canard unit (forebody and canards) loads and the whole loads, thus enabling the identification of the canard-main-body interactions. Mach number of the tests was 0.8, and angle of attack was varied between −6 and 14 deg. The canards were installed at the + and x positions and at deflection angles of 0, 6, and 12 deg (leading edge up). Additional details, including accuracy of the data, are given in Ref. 1.

Characteristics of Canard-Body Configurations

Typical test results of the canard unit, mounted on body b-B20, and of the total configuration are presented in Figs. 3 and 4 for the + and the x positions, respectively. The reference length and area are forebody diameter and cross-sectional area, respectively. The reference for pitching moment is the interface between the forebody and the main bodies, as indicated in Fig. 1. The reference quantities

Presented as Paper 99-3146 at the AIAA 17th Applied Aerodynamics Meeting, Norfolk, VA, 28 June–1 July 1999, and as Paper 2000-4525 at the 18th Applied Aerodynamics Meeting, Denver, CO, 14–17 August 2000; received 20 June 2000; revision received 1 April 2001; accepted for publication 23 April 2001.

*Visiting Professor, Department of Aerospace Engineering; currently Adjunct Research Associate, Faculty of Aerospace Engineering, Technion—Israel Institute of Technology, 32000 Haifa, Israel; AsherS@aerodyne.technion.ac.il. Associate Fellow AIAA.

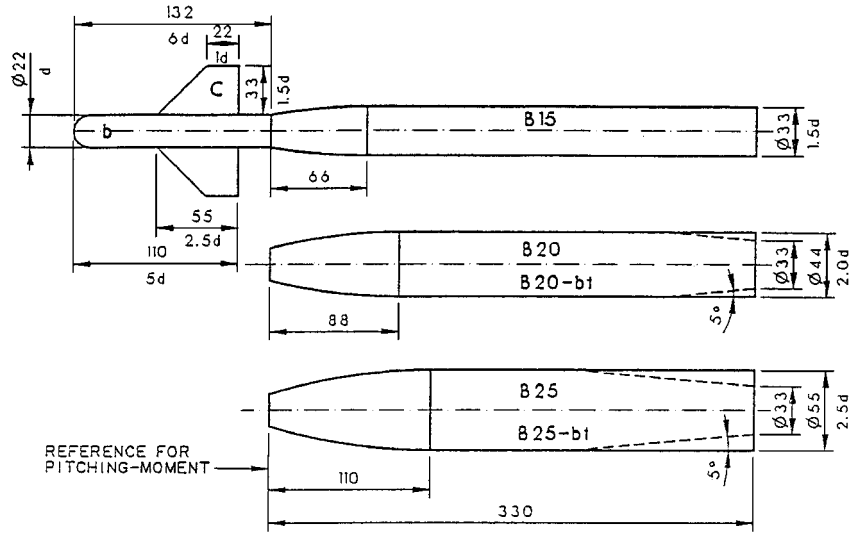

Fig. 1 Schematic of the model and designation of the modules.

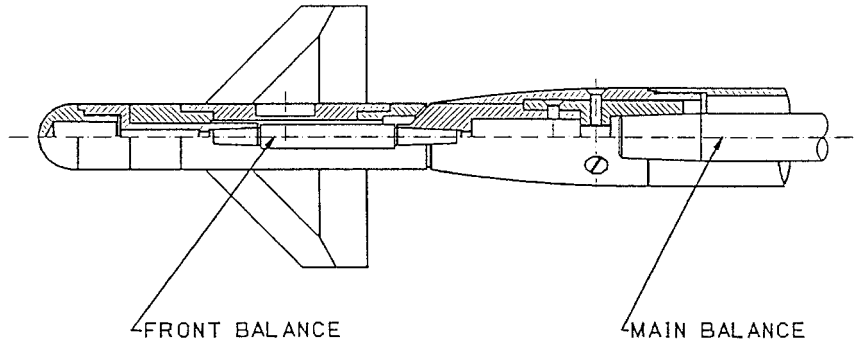

Fig. 2 General assembly of configuration b-C00-B15.

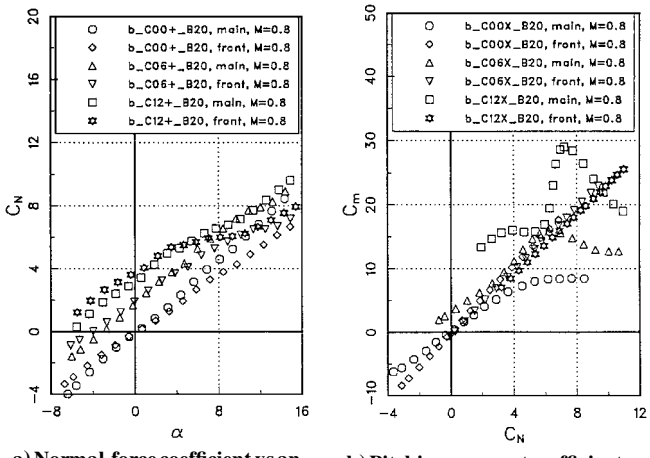

a) Normal-force coefficient vs angle of attack

b) Pitching-moment coefficient vs normal-force coefficient

Fig. 3 Test results of the canard unit and the whole configuration at the + position.

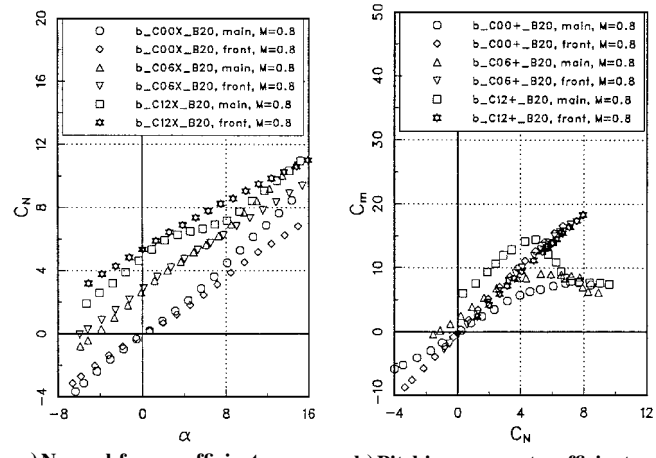

a) Normal-force coefficient vs angle of attack

b) Pitching-moment coefficient vs normal-force coefficient

Fig. 4 Test results of the canard unit and the whole configuration at the *x* position.

are common to all configurations. The coefficients obtained by each balance are presented as a function of the appropriate angle of attack. The ratio of forebody to main body angles of attack, which results from the bending of the front balance, range between 1.02 and 1.04, depending on canard deflection. The normal-force curve slopes of the whole configuration are slightly larger than those of the canard unit. The nonlinear components of the normal-force curves of the configuration are larger than those of the canard unit, indicating the contribution of the main body. When the canards are deflected, the normal-force coefficients of the configuration, at zero angle of attack, are lower than those of the canard unit. As angle of attack increases, the normal-force curves of the configuration cross over those of the canard unit, and increase without saturation. For undeflected canards the initial slopes of the pitching-moment curves (C_m vs C_N) of the configuration are smaller than those of the canard unit. The smaller slopes indicate a more rearward center-of-pressure location because of the contribution of the main bodies. The pitching moments of deflected canards, at zero angle of attack, are larger than those of the canard units. Also, whole pitching-moment coefficients at zero normal force are positive, indicating the existence

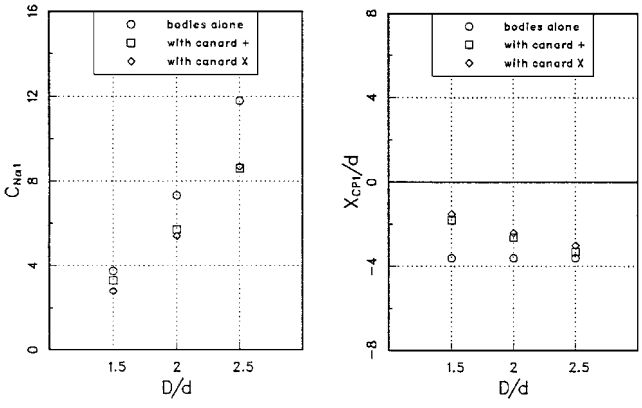

a) Normal-force curve slope **b) Center-of-pressure location**

Fig. 5 Stability derivatives of the plain main bodies in presence of the canard.

of moment couples. As the normal-force coefficient increases, the center-of-pressure location of the configuration, indicated by the ratio C_m/C_N, moves rearward as a result of nonlinear contribution of the main body. Similar results were obtained with all other bodies. The effects already mentioned are more pronounced as D/d increases.

Canard on Main Body Influences

The contributions of the plain main bodies (main bodies without boattails) to stability derivatives were obtained by applying Eqs. (1) to the data of the configurations with nondeflected canards:

$$C_{N_\alpha 1} = C_{N_\alpha m} - C_{N_\alpha f} \tag{1a}$$

$$C_{m_\alpha 1} = C_{m_\alpha m} - C_{m_\alpha f} \tag{1b}$$

$$x_{\mathrm{cp}1}/d = C_{ml}/C_{\mathrm{Nl}} \tag{1c}$$

The results are plotted in Fig. 5, together with those obtained for the bodies alone. It is apparent that the normal-force curve slopes of the thickenings of the main bodies are reduced by the presence of the canard. The center-of-pressure locations of this contribution are more forward, relative to the case of bodies alone. The shift of the center of pressure indicates that the download, that reduces $C_{N_\alpha 1}$, acts more aft than the center of pressure of the thickenings of the bodies alone.

A canard on main body influence factor is defined by

$$I_\alpha = \frac{C_{N_\alpha 1}(b - C - B^*)}{C_{N_\alpha 1}(b - B^*)} - 1 \tag{2}$$

The average value, based on the data presented in Fig. 5 (one irregular datum excluded), is

$$I_\alpha = -0.25$$

As mentioned earlier, the whole normal-force coefficients caused by canard deflection at zero angle of attack, obtained by the main balance, are smaller than those of the canard unit, obtained by the front balance. The differences are shown in Fig. 6. A canard on main body influence factor caused by canard deflection is defined by

$$I_\delta = \Delta C_{\mathrm{Nl}}/C_{\mathrm{Nf}} \tag{3a}$$

where

$$\Delta C_{\mathrm{Nl}} = C_{\mathrm{Nm}} - C_{\mathrm{Nf}} \qquad \text{at} \qquad \alpha = 0 \tag{3b}$$

The dependence of I_δ on diameter ratio is discussed in the next section.

Canard on Boattail Influences

The contributions of the boattails to the normal-force curve slopes, in the presence of the canard, were obtained by subtracting the stability derivatives of configurations having plain bodies from those of matching configurations having boattails. The findings are summarized in Table 1.

Table 1 Normal-force curve slope of the boattails in presence of the canard

Configuration	b-C-B20bt[a]	b-C-B25bt
With canards at +	−2.13	−4.63
With canards at x	−2.45	−4.75
Bodies alone	−4.14	−7.80

[a]b = forebody; C = canard; B = main body; bt = boattail.

Table 2 Deflected canard on boattail influence factor

Configuration	b-C-B20bt[a]	b-C-B25bt
Canards at +	0.040	0.070
Canards at x	0.046	0.102

[a]b = forebody; C = canard; B = main body; bt = boattail.

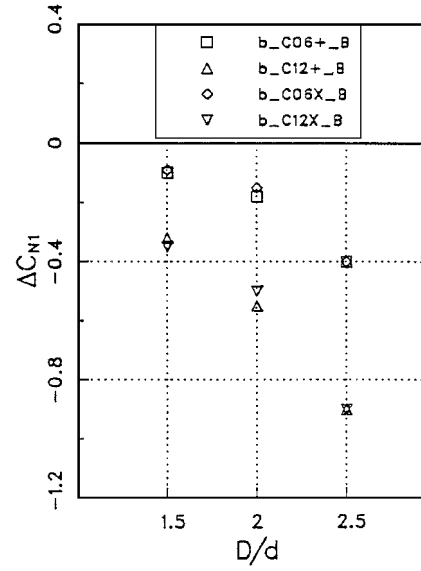

Fig. 6 Aerodynamic loads induced by canard deflection on the plain main bodies.

The presence of the canards considerably reduces, in absolute value, the contributions of the boattails to normal-force curve slopes. Similar to the first interaction, a canard on boattail influence factor is defined by

$$I_{\alpha\mathrm{bt}} = \frac{C_{N_\alpha \mathrm{bt}}(b - C - B^*\mathrm{bt})}{C_{N_\alpha \mathrm{bt}}(b - B^*\mathrm{bt})} - 1 \tag{4}$$

The average value, based on the data given in Table 1, is

$$I_{\alpha\mathrm{bt}} = -0.42$$

The total normal-force coefficients of configurations with deflected canards and boattails, at zero angle of attack, are larger than those of the matching plain configurations. Similar to the second influence factor, a deflected canard on boattail influence factor is defined by

$$I_{\delta\mathrm{bt}} = \Delta C_{\mathrm{Nbt}}/C_{\mathrm{Nf}} \tag{5a}$$

where

$$\Delta C_{\mathrm{Nbt}} = C_{\mathrm{Nm}}(b - C - B^*\mathrm{bt}) - C_{\mathrm{Nm}}(b - C - B^*) \qquad \text{at} \qquad \alpha = 0 \tag{5b}$$

The experimentally obtained average values (between 6- and 12-deg canard deflections) are given in Table 2.

Analysis

Review of the P-N-K Methodology

Analysis of the effect of a vortex system created by forward lifting surfaces on afterbodies is included in the Pitts, Nielsen, and Kaattari (P-N-K) formulation of component buildup (CBU) methodology.[2] This reference modeled each lifting surface by a horseshoe vortex. The external trailing vortex is a free vortex, whereas the internal vortex is an image of the external one, which satisfies the tangency conditions on the body. The relationship between the circulation and the lift produced by a planar canard is

$$\Gamma = \tfrac{1}{4} U S_R C_{Lc}/(f-g)_c \tag{6}$$

For slender fins the source of the trailing vortex is at

$$f_c = r_c + (\pi/4)(s-r)_c \tag{7}$$

The location of the image vortices is given by

$$g = fr^2/(f^2+h^2) \tag{8a}$$

$$h_i = hr^2/(f^2+h^2) \tag{8b}$$

The net lift carried on a body section, located downstream of the canards, is

$$\Delta L = 2\rho U \Gamma \Delta(f-g) \tag{9}$$

where $\Delta(f-g)$ is the change of $(f-g)$ along that body section. The nondimensional form of Eq. (9) is

$$\Delta C_L = (4\Gamma/US_R)\Delta(f-g) \tag{10}$$

With regard to the location of the free vortices, the authors of Ref. 2 mention the "step by step" analysis (vortex tracking) of Rogers.[3] However, their own analysis assumes that the free vortices are convected in the direction of the free flow. This approximation was applied to the present configurations. It was found that the estimated interactions were much larger, in absolute values, than experimentally observed. This finding led to a desire to refine the analysis.

Present Methodology

To apply Eq. (10), there is a need to know the trajectories of the free vortices downstream of the canard trailing edge. Vortex tracking was developed for the study of vortex roll up (e.g., Rogers[3] or Spreiter and Sacks[4]) and for the analysis of wing-tail interaction (e.g., Edwards and Hikido[5]). The analysis by Refs. 3–5 considered two contributions to the displacement of the vortices: the crossflow over the body at angle of attack and the mutual induction of the vortices. Slender-body theory was used for the former and two-dimensional vortex theory for the later. Nielsen[6] and Hemsch[7] provide additional details and references. Vortex trackers are being used in several CBU codes, e.g., Portnoy[8] or Lesieutre et al.[9] These trackers require numerical integration along the body.

The emphasis of this work is on the effect of variable body diameter at small angles of attack. It is expected that in this case the changing diameter will dominate the lateral displacement of the vortices. Thus, an approximate approach was sought, which will yield an analytical solution, rather than a need for numerical integration.

According to subsonic slender body theory, i.e., Ashley and Landahl[10] or Katz and Plotkin,[11] the local source strength, representing a slender body at zero angle of attack, is

$$\frac{\sigma}{U} = \frac{\mathrm{d}S}{\mathrm{d}x} = \frac{2\pi r\,\mathrm{d}r}{\mathrm{d}x} \tag{11}$$

The radial velocity component induced by the source, at small distances from the axis, is approximately

$$\frac{q_r}{U} = \left(\frac{1}{2\pi R}\right)\frac{\mathrm{d}S}{\mathrm{d}x} = \left(\frac{r}{R}\right)\frac{\mathrm{d}r}{\mathrm{d}x} \tag{12a}$$

Because free vortices are aligned with streamlines

$$\frac{q_r}{U} = \frac{\mathrm{d}R}{\mathrm{d}x} = \left(\frac{r}{R}\right)\frac{\mathrm{d}r}{\mathrm{d}x} \tag{12b}$$

Integration of Eq. (12b) yields

$$R^2 - r^2 = R_c^2 - r_c^2 \qquad \text{(a constant)} \tag{13}$$

The physical interpretation of Eq. (13) is that at zero angle of attack the free vortices coincide with the outer surface of a hollow stream tube, whose inner surface is the body.

Validation

Substituting Eq. (6) into Eq. (10) yields

$$\Delta C_L = \frac{C_{LC}\Delta(f-g)}{(f-g)_c} \tag{14a}$$

$$\Delta C_{L_\alpha} = \frac{C_{L_\alpha C}\Delta(f-g)}{(f-g)_c} \tag{14b}$$

Ignoring the small differences between C_L and C_N, the four influence coefficients become

$$I_\alpha = \frac{C_{N_{\alpha c}}}{C_{N_{\alpha l}}(b-B)}\frac{\Delta(f-g)_1}{(f-g)_c} \tag{15a}$$

$$I_\delta = \frac{\Delta(f-g)_1}{(f-g)_c} \tag{15b}$$

$$I_{\alpha\mathrm{bt}} = \frac{C_{N_{\alpha c}}}{C_{N_{\alpha\mathrm{bt}}}(b-B)}\frac{\Delta(f-g)_{\mathrm{bt}}}{(f-g)_c} \tag{15c}$$

$$I_{\delta\mathrm{bt}} = \frac{\Delta(f-g)_{\mathrm{bt}}}{(f-g)_c} \tag{15d}$$

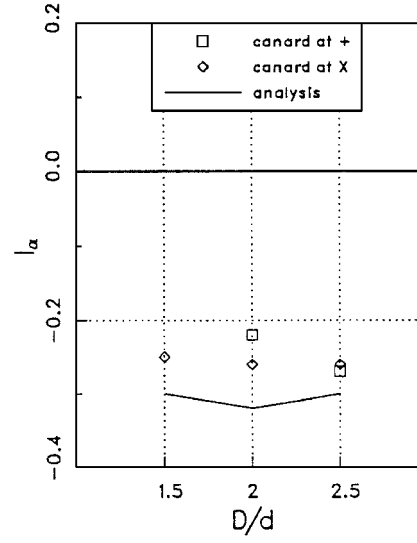

Fig. 7 Canard on main bodies influence factor.

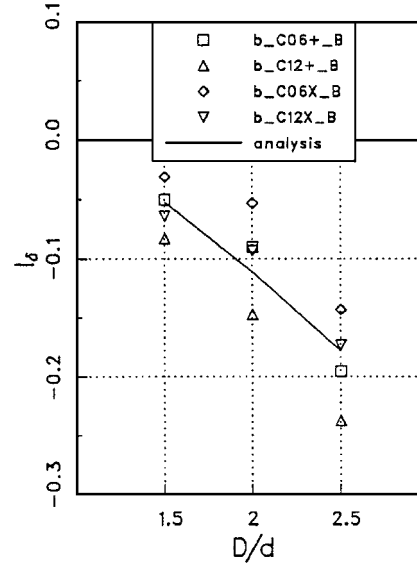

Fig. 8 Deflected canard on main bodies influence factor.

The ratio $\Delta(f-g)/(f-g)_c$, which is the normalized change of the lateral distance between the trailing vortices and their images, is calculated using Eq. (13). The results for the thickenings and the boattails of the present geometries are summarized in Table 3. For near zero angles of attack and weak vortices, the influence coefficients are independent of the roll position. A similar analysis, assuming that the free canard vortices trail in the direction of the freestream, gave values that are two to three times larger than those given in Table 3. The large difference emphasizes the importance of tracking the vortices in the analysis of the interactions.

I_α Evaluation

The experimentally obtained values were obtained by applying Eq. (2) to the data presented in Fig. 1. The analytical prediction was obtained using Eq. (15a), experimental data for the normal-force curve slopes of the canard unit and of the thickening of the main bodies, and the calculated vortex lateral distance parameter given in Table 3. Figure 7 is a comparison between test data and analysis. The average calculated value is -0.31, namely 24% larger, in absolute value, than the average experimental value of -0.25.

I_δ Evaluation

The experimental data were obtained using Eq. (3a), the data summarized in Fig. 2, and experimentally obtained characteristics of the canard unit. The analytical values, according to Eq. (15b), are taken from Table 3. Figure 8 compares the results of the analysis with those of the test. It is apparent that the analytical curve passes in the middle of the test data.

$I_{\alpha bt}$ Evaluation

The test data were obtained by applying Eq. (4) to the data given in Table 1. The analysis uses Eq. (15c) and experimental data for the characteristics of the canard unit. The average analytical value is -0.34, namely 19% smaller, in absolute value, than the experimentally obtained average value of -0.42.

$I_{\delta bt}$ Evaluation

A comparison of Table 2 and the bottom line of Table 3 shows that the analysis overestimates the experimentally obtained data by an average of 44%.

A more detailed analysis that accounts for the differences between forebody and main body angles of attack was also carried out. It was found that predictions by the refined analysis are close to those obtained by the present method.

Table 3 Change of vortex lateral distance along the models

	D/d		
Change	1.5	2.0	2.5
$\Delta(f-g)_1/(f-g)_c$	-0.052	-0.110	-0.176
$\Delta(f-g)_{bt}/(f-g)_c$	——	0.060	0.124

Applications

The basic prediction tool was the 1997 version of the Missile Datcom code (M-Datcom).[12] It was used to obtain the longitudinal characteristics of the selected configurations and of their components. The pertinent parts of Eqs. (15) were used to account for the subject interactions, which are not considered by the code. The M-Datcom code assumes, after Ref. 2, that the free vortices trail in the direction of the freestream. The present analysis considers the lateral displacement of these vortices as they trail along the bodies. A change in the lateral position of the vortices also affects the tail interference factor, which determines the contributions of the tail caused by canard vortices. This creates an additional indirect interaction, which is also taken into account in the analysis. The modified results of the M-Datcom are entitled corrected.

The reference length and area used in this chapter are maximum body diameter and cross-sectional area, respectively. These reference quantities match those used by the authors whose data are used for comparison.

Canard-Body-Flare Missile

Spearman and Robinson[13] tested a canard-body-flare missile model at high supersonic Mach numbers, at angles of attack, and canard deflections up to 20 deg. A schematic of their research configuration is depicted in Fig. 9. The M-Datcom computational model is slightly different from the actual geometry: 1) The nose of the computational model is a slightly blunted tangent ogive. It maintains the bluntness radius and the radius at midroot chord station of

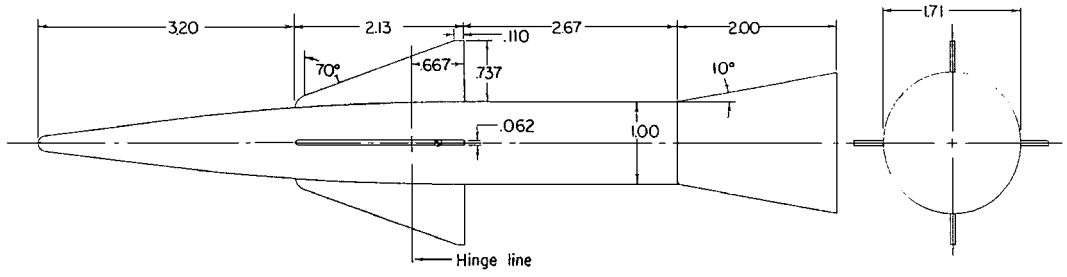

Fig. 9 Schematic of canard-body-flare configuration.[13]

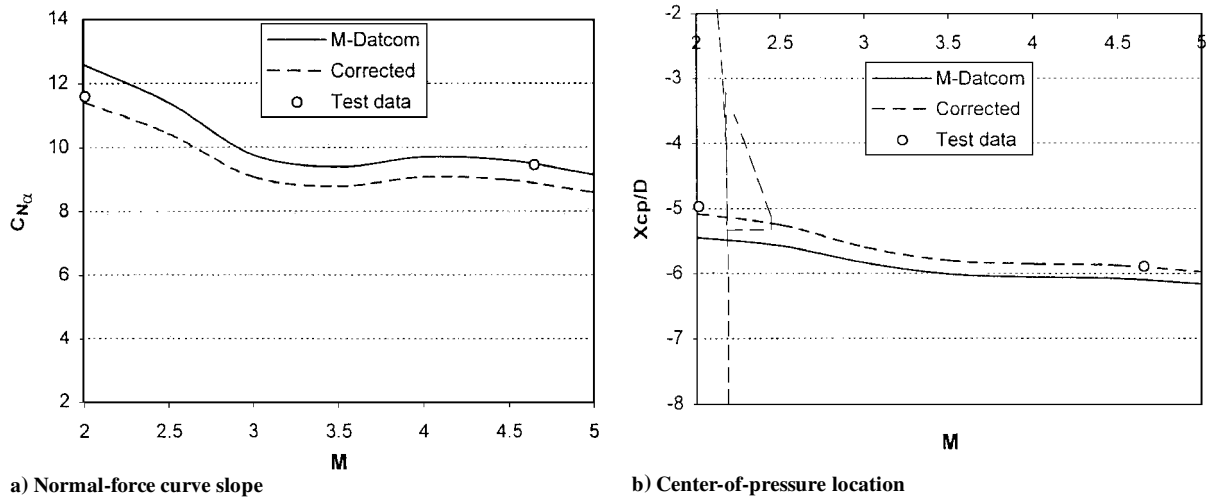

a) Normal-force curve slope **b) Center-of-pressure location**

Fig. 10 Comparison of longitudinal stability derivatives of canard-flare-body configuration.

the actual model. 2) The computational canard model is trapezoidal, maintaining the same inclusive span and exposed area as the actual planform. The analysis and the comparisons were done for Mach numbers up to 5.0.

The lateral positions of the canard trailing and image vortices, in center-body diameters, are given in Table 4.

Test data were obtained from Fig. 7 of Ref. 13. The maximum probable error given in Ref. 13 is ± 0.11 in C_N and ± 0.13 in C_m, for $M = 4.64$ and about 10% better at $M = 2.01$. Comparisons between M-Datcom prediction, corrected analysis and test data are presented in Figs. 10 and 11. The "saddle" in the calculated curves is attributed to the contribution of the canards, which is obtained from a database. The correction, which accounts for the download acting on the flare caused by canard vortices, decreases the normal-force curve slope by about 11% at $M = 2.0$ to 7.4% at $M = 5.0$. The reduction of the normal-force caused by canard deflection stability derivative is

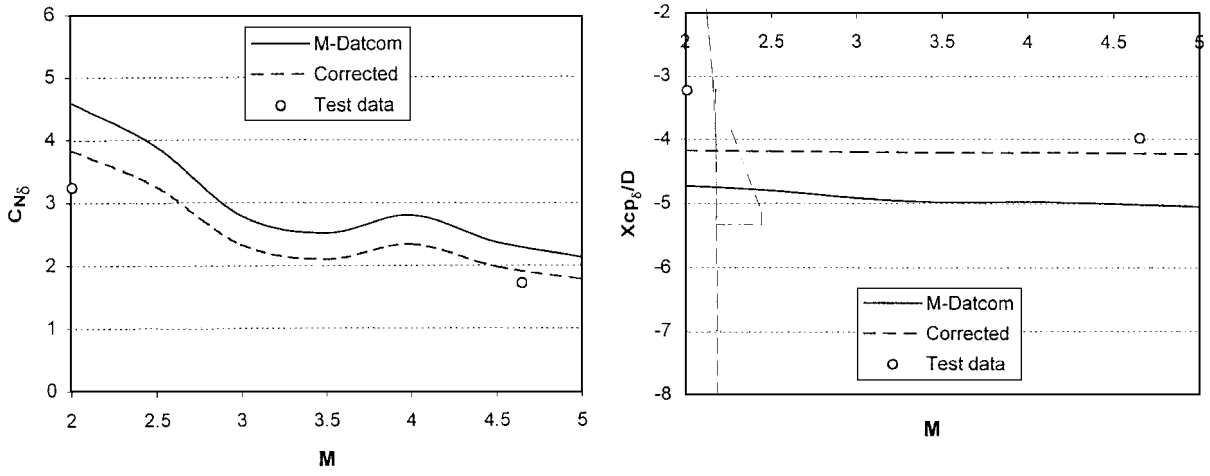

a) Normal force caused by canard deflection **b) Center-of-pressure location**

Fig. 11 Comparison of control stability derivatives of canard-flare-body configuration.

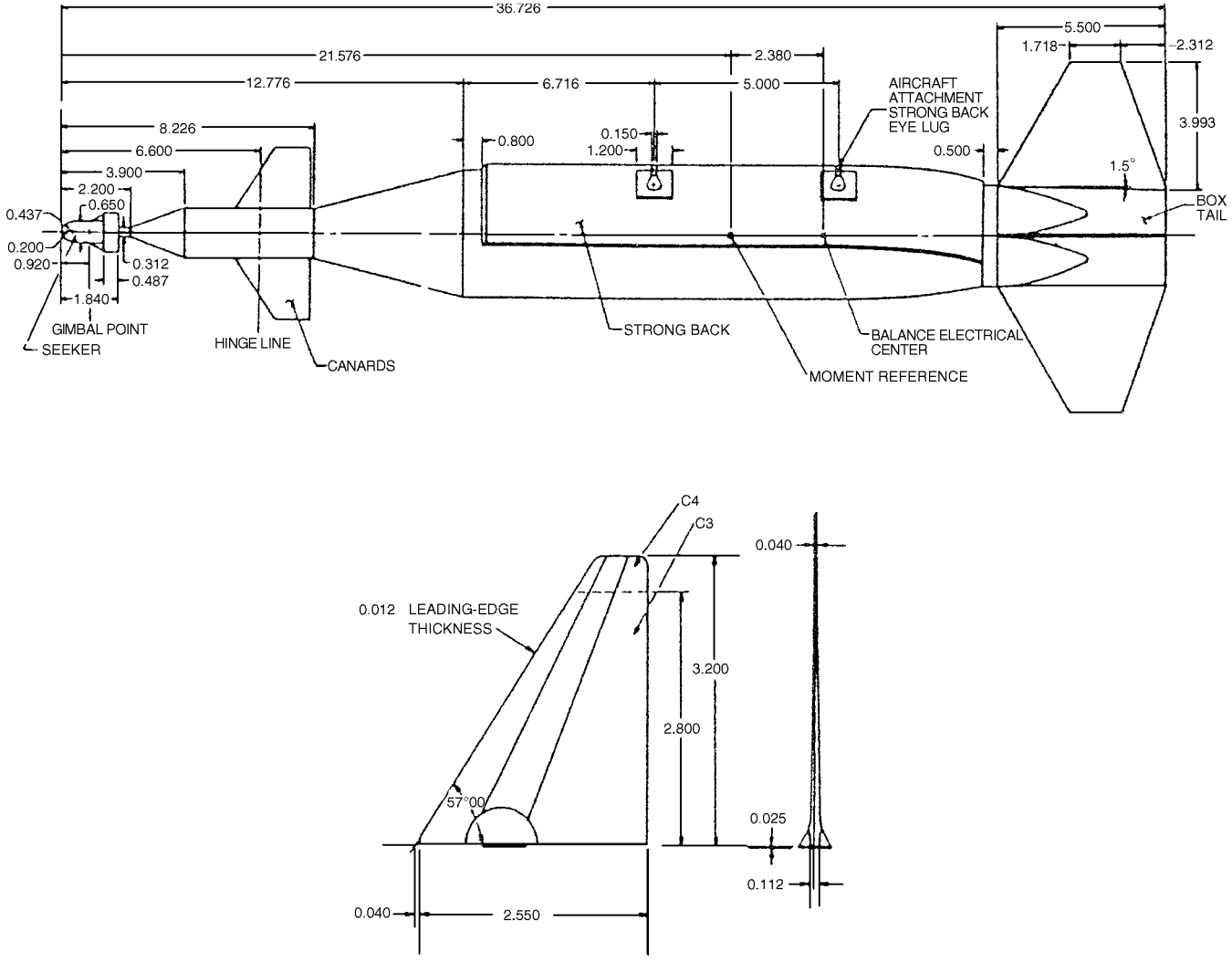

Fig. 12 Schematic of the wind-tunnel model of Pavestorm I.[14]

16.5% and is independent of Mach number. The corrected computational values are in better agreement with the test data, except for the normal-force curve slope at $M = 4.65$. The correction shifts the center of pressures forward about $0.36D$ at $M = 2.0$ to $0.18D$ at $M = 5.0$. The corrected center-of-pressure location is in very good agreement with the data. The center of pressure caused by canard deflection, as predicted by the M-Datcom, is very close to that of the isolated canards. The correction shifts this center of pressure forward between $0.5D$ at $M = 2.0$ and $0.8D$ at $M = 5$ and improves the agreement with test data.

Pavestorm I

The Pavestorm missile features a canard unit, which is mounted on a thin forebody, a thick main body, a boattail, and a tail. Smith[14] tested this configuration at transonic Mach numbers. A schematic of his test model is shown in Fig. 12. Canard C3, which has the middle size, was selected for the present study.

The computational model contains three small deviations from the actual configuration: 1) The actual nose (cone-cylinder-flare) was replaced by a cone having a fineness ratio of 2.44. Modeling the nose as a cone enables the use of the first option of analysis, which uses a database. This option has the advantage of taking into account the lift carryover on the main body. The selected fineness ratio ensures that the body diameter at the location of the center of the canard root chord is equal to the actual diameter; 2) The actual afterbody (boattail-box tail) was represented by a conical boattail. The computational model base diameter was calculated such that the normal-force curve slope of the equivalent base diameter will equal that of the actual box tail, based on slender body theory. According to this theory, i.e., Nielsen,[6] the normal-force curve slope of a square body is 2.47. Thus

$$\pi / 2d_{\text{be}}^2 = 2.47c^2 \tag{16}$$

Equation (16) gives $d_{\text{be}} = 1.25c$; 3) The root chord of the tail is shifted outward so that it matches the computational model of the boattail. The inclusive span of the tail is maintained. A comparison between the actual body contour and the computational model is depicted in Fig. 13. The radial location of the canard vortices at selected body stations, in body diameters, is given in Table 5.

The moment arms are $l_1/d = 2.73$ and $l_{\text{bt}}/d = 2.41$ for the thickening of the forebody and for the boattail, respectively. This gives the net effects

$$\Delta C_L = -0.043 C_{\text{LC}} \tag{17a}$$

$$\Delta C_m = -0.673 C_{\text{LC}} \tag{17b}$$

Table 4 Lateral positions of the canard vortices canard-body-flare missile[13]

Station	f	g	$(f-g)$	$\Delta(f-g)$	$\Delta(f-g)/(f-g)_c$
T.E.[a] of canard	1.08	0.23	0.85	——	——
Base of flare	1.28	0.57	0.71	−0.14	−0.165

[a]T.E. = trailing edge.

Table 5 Lateral positions of the canard vortices: Pavestorm I[14]

Station	f	g	$(f-g)$	$\Delta(f-g)$	$\Delta(f-g)/(f-g)_c$
T.E.[a] of canard	0.741	0.052	0.689	——	——
Main body	0.871	0.286	0.585	−0.104	−0.151
Base of boattail	0.772	0.113	0.659	0.074	0.108

[a]T.E. = trailing edge.

Configurations B1-C3 (body-canard) and B1-C3-T1 (body-canard-tail) were analyzed with lifting surfaces at both the + and x positions and for nondeflected and 5.5 deg deflected canards. The direct corrections use Eqs. (15), with calculated values for the characteristics of the canard unit. Table 5 shows that the radial location of the free vortices at the tail zone is slightly larger than that at their origin at the canard trailing edge. Chart 7 of Ref. 2 was used to estimate the effect of this change of the lateral position on the tail interference factor. It was found that the lateral shift increases the interference factor by 3.4% in absolute value. The normal-force curve slope of the tail unit, alone and in the presence of the canards, was obtained by subtracting the normal-force curve slope of the body alone from that of the body-tail and the body-tail-canard configurations. The difference between the two cases is the contribution of the tail caused by canard vortices (downwash). The additional correction was obtained by increasing this contribution by 3.4%, as just mentioned.

The accuracy of the data given in Ref. 14 for $M = 0.65$ is 0.04 for C_N and 0.02 for C_m. The accuracy improves as Mach number

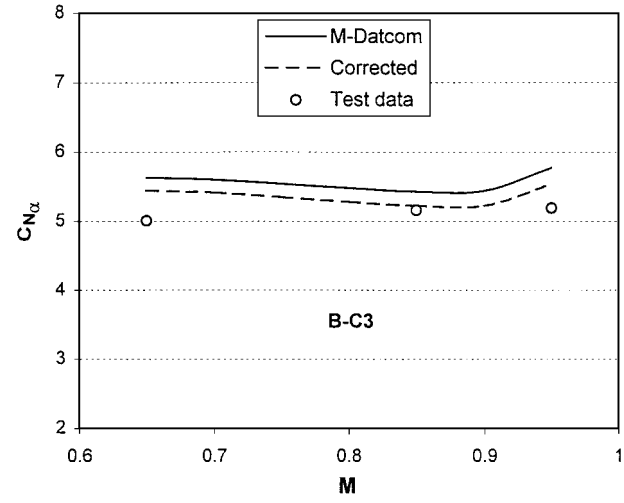

a) Normal-force curve slope

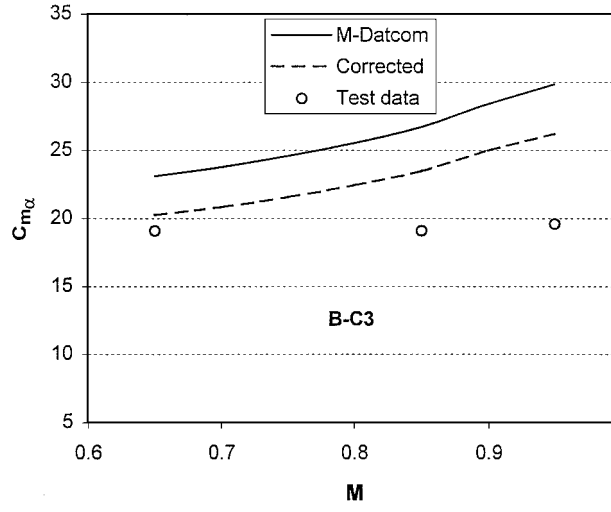

b) Pitching-moment curve slope

Fig. 14 Comparison of the stability derivatives of configuration B1-C3.

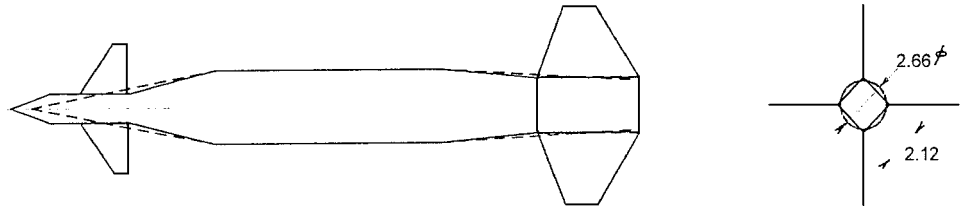

Fig. 13 Comparison between body outline and the computational model of Pavestorm I.

increases. The experimentally obtained stability derivatives were estimated by manual fitting straight lines to the graphical data at small angles of attack. The pitching-moment curves of the complete configuration (B1-C3-T1) feature strong nonlinearity (S curve) around zero angle of attack. Thus, the experimentally obtained pitching-moment curve slope was not evaluated for this configuration. Also, the net normal-force coefficient caused by canard deflection of the whole configuration is very small and compares with the accuracy of the data reduction. Thus, this coefficient too is not being compared.

Comparisons of calculated and experimentally obtained longitudinal characteristics of configuration B1-C3 are shown in Fig. 14. Test data with nondeflected canards are available for surfaces at the + position. It is apparent that the correction improves the agreement with test data for both stability derivatives. The normal force and pitching moment caused by canard deflection of 5.5 deg are presented in Fig. 15. The calculated normal-force coefficient is considerably larger than the test data. The present correction has the right trend, but it is much smaller than the remaining gap. The matching pitching-moment curve with canards in the + position is in very good agreement with the data. In the *x* orientation the agreement is good at Mach number of 0.65, but a gap develops as Mach number increases.

The calculated and experimentally obtained normal-force curve slopes of configuration B1-C3-T1 are presented in Fig. 16. For this configuration the M-Datcom results overestimate the test data, whereas the corrected results are in very good agreement with it. Figure 17 brings a comparison between calculated and experimentally obtained data for the pitching moment caused by canard deflection of 5.5 deg. In this case the indirect correction offsets about 10% of the direct correction. The findings are very similar to those found for configuration B1-C3, namely, good agreement with the test data for surfaces in the + orientation and at $M = 0.65$ also for the *x* position. At Mach numbers larger than 0.65 and *x* position there remains an unexplained gap between analysis and test data.

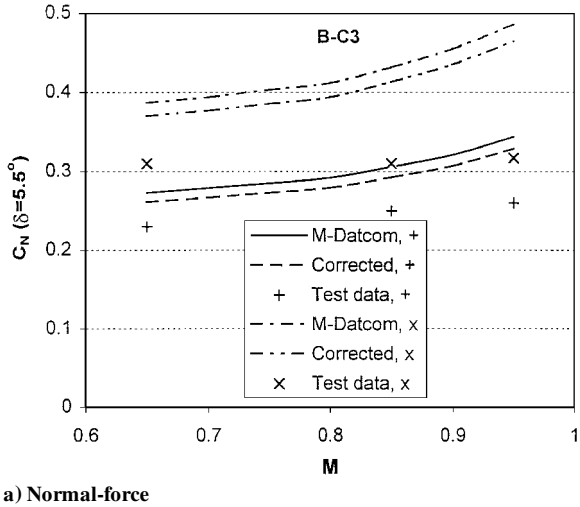

a) Normal-force

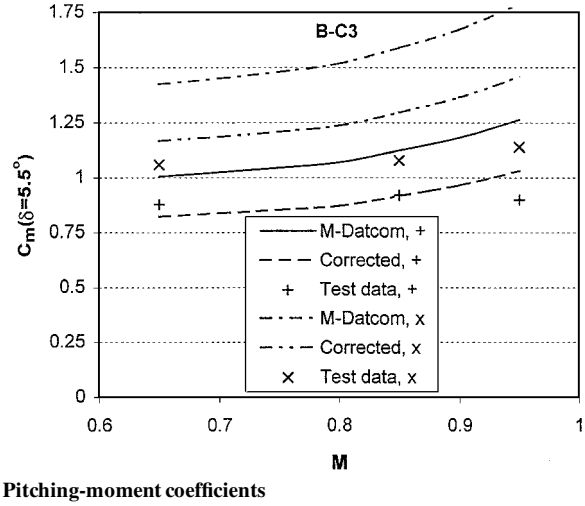

b) Pitching-moment coefficients

Fig. 15 Comparison of the control loads caused by 5.5-deg canard deflection of configuration B1-C3.

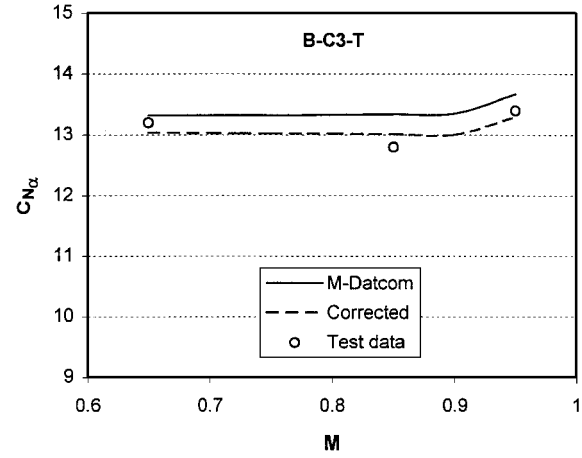

Fig. 16 Comparison of the normal-force curve slope of configuration B1-C3-T1.

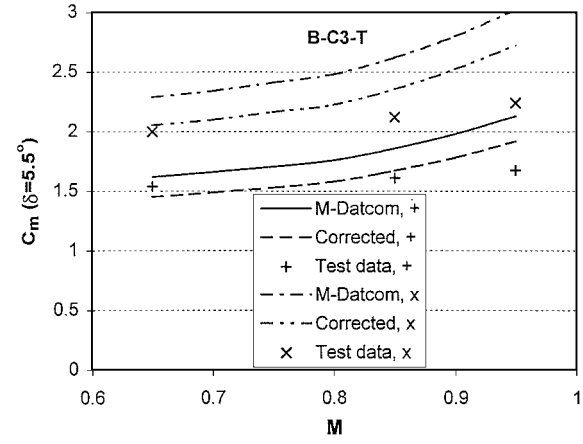

Fig. 17 Comparison of the pitching-moment coefficient caused by 5.5-deg canard deflection for configuration B1-C3-T1.

Conclusions

The wind-tunnel test results of Ref. 1 were processed, and four interactions between a canard and thick bodies were identified: effects of the canard on the thickenings of the main bodies and on the boattails as a function of angle of attack and canard deflection.

An approximate vortex tracker, which is based on slender body theory, is used to estimate the change of the radial location of the canard trailing vortices along the body at zero angle of attack.

The effects of the canard unit on bodies were analyzed, using the present vortex tracker and the Pitts, Nielsen, and Kaattari[2] method. The calculated results agree well with the experimentally obtained data, except for the deflected canard on boattail influence factor where the gap is large.

Several configurations were analyzed without and with the subject interactions. It is shown that including the contributions of the interactions between the canard vortex wakes and the bodies improves the agreement between results of component buildup estimates and test data.

Incorporation of the new method in CBU codes, such as the M-Datcom, would improve the prediction of canard-controlled configurations that feature thick bodies.

References

[1] Sigal, A., and Victor, M., "Interactions Between a Canard and Thick Bodies: Characteristics of the Components," *Journal of Spacecraft and Rockets*, Vol. 38, No. 6, 2001, pp. 882–887.

[2]Pitts, W. C., Nielsen, J. N., and Kaattari, G. E., "Lift and Center of Pressure of Wing-Body-Tail Combinations at Subsonic, Transonic, and Supersonic Speeds," NACA Rept. 1307, 1957.

[3]Rogers, A. W., "Application of Two-Dimensional Vortex Theory to the Prediction of Flow Behind Wings of Wing-Body Combinations at Subsonic and Supersonic Speeds," NACA TN 3227, 1954.

[4]Spreiter, J. R., and Sacks, A. H., "A Theoretical Study of the Aerodynamics of Slender Cruciform-Wing Arrangements and their Wakes," NACA Rept. 1296, 1957.

[5]Edwards, S., and Hikido, A., "A Method for Estimating the Rolling Moment Caused by Wing-Tail Interference for Missiles at Supersonic Speeds," NACA RM A53H18, 1953.

[6]Nielsen, J. N., *Missile Aerodynamics*, Nielsen Engineering and Research, Inc., Mountain View, CA, 1988, pp. 34–40, 144–168, 363–373.

[7]Hemsch, M. J., "Component Build-Up Method for Engineering Analysis of Missiles at Low-to-High Angles of Attack," *Tactical Missile Aerodynamics: Prediction Methodology*, edited by M. R. Mendenhall, Vol. 142, Progress in Astronautics and Aeronautics, AIAA, Washington, DC, 1992, pp. 115–169.

[8]Portnoy, H., "Calculation of the Aerodynamic Forces and Moments on Complex Cruciformed-Winged Missile Configurations up to Intermediate Angle of Attack," *Israel Journal of Technology*, Vol. 23, Nos. 1–2, 1986, pp. 33–46.

[9]Lesieutre, D. J., Mendenhall, M. R., Nazario, S. M., and Hemsch, M. J., "Aerodynamic Characteristics of Cruciform Missiles at High Angles of Attack," AIAA Paper 87-0212, Jan. 1987.

[10]Ashley, L., and Landahl, M., *Aerodynamics of Wings and Bodies*, Addison Wesley Longman, Reading, MA, 1965, pp. 99–107.

[11]Katz, J., and Plotkin, A., *Low-Speed Aerodynamics*, McGraw–Hill, New York, 1991, pp. 225–233.

[12]Blake, W. B., "Missile Datcom User's Manual—1997 Fortran 90 Revision," U.S. Air Force Research Lab., Air Vehicle Directorate, AFRL-VA-WP-1998-3009, Wright–Patterson AFB, OH, Feb. 1998.

[13]Spearman, M. L., and Robinson, R. B., "Longitudinal Stability and Control Characteristics at Mach Numbers 2.01, 4.65, and 6.8 of Two Hypersonic Missile Configurations, One Having Low-Aspect-Ratio Cruciform Wings With Trailing-Edge Flaps and One Having a Flared Afterbody and All-Movable Controls," NASA TM X-46, Sept. 1959.

[14]Smith, D. K., "Effect of Several Canard Sizes on the Static Stability, Performance, and Trim Characteristics of the Pavestorm I Munition System at Transonic Speeds," Arnold Engineering Development Center, AEDC-TR-72-67, Arnold AF Station, TN, May 1972.

M. S. Miller
Associate Editor